Available online at www.sciencedirect.com
SCIENCE DIRECT®
Journal of Catalysis 231 (2005) 279–291
JOURNAL OF CATALYSIS
www.elsevier.com/locate/jcat

In situ investigations of the bulk structural evolution of vanadium-containing heteropolyoxomolybdate catalysts during thermal activation

Thorsten Ressler [a,*], Olaf Timpe [a], Frank Girgsdies [a], Julia Wienold [b], Thomas Neisius [c]

[a] *Department of Inorganic Chemistry, Fritz-Haber-Institute of the MPG, Faradayweg 4-6, D-14195 Berlin, Germany*
[b] *HASYLAB at DESY, Notkestr. 85, D-22603 Hamburg, Germany*
[c] *European Synchrotron Radiation Facility, BP 220, F-38043 Grenoble cedex, France*

Received 19 October 2004; revised 20 December 2004; accepted 10 January 2005

Available online 17 March 2005

Abstract

The bulk structural evolution of a vanadium-containing heteropolyoxomolybdate (HPOM), $H_4[PVMo_{11}O_{40}] \times 13H_2O$, with vanadium substituting for Mo in the Keggin ion, was studied under reducing (propene) and partial oxidation reaction conditions (propene and oxygen) by in situ X-ray diffraction (XRD) and X-ray absorption spectroscopy (XAS) combined with mass spectrometry. During treatment in propene, the loss of crystal water in the temperature range from 373 to 573 K was followed by a partial decomposition, reduction of the average Mo valence, and formation of a characteristic cubic HPOM at 573 K. This behavior is similar to the structural evolution of $H_3[PMo_{12}O_{40}] \times 13H_2O$ during treatment in propene. The formation of cubic $Mo_x[PVMo_{11-x}O_{40}]$ with Mo centers on extra Keggin framework positions and V centers remaining in the lacunary Keggin ion coincides with the onset of catalytic activity at $\sim$ 573 K. Detailed investigations of the local structure around the vanadium centers in $Mo_x[PVMo_{11-x}O_{40}]$ have made it possible to propose a model for the geometric structure of the active site in Mo- and V-containing metal oxide catalysts. The cubic $Mo_x[PVMo_{11-x}O_{40}]$ phase prepared from $H_4[PVMo_{11}O_{40}] \times 13H_2O$ is stable in propene and oxygen up to $\sim$ 620 K and exhibits an onset of activity at $\sim$ 573 K. This onset of activity is correlated to characteristic changes in the average local Mo structure, indicating a reversible transition from the reduced state of the active site in $Mo_x[PVMo_{11-x}O_{40}]$ to an oxidized state under propene oxidation reaction conditions.

Keywords: In situ; Structure–activity relationships; Molybdenum; XAFS spectroscopy; Polyoxometalates; Partial oxidation; Vanadium; Heteropoly acids

1. Introduction

The development of more active and selective catalysts for partial oxidation of alkanes and alkenes is extensively pursued in both industrial and academic research. Molybdenum oxide based-catalysts for partial oxidation reactions have long been studied and industrially employed [1]. Recently, mixed $MoVNbTeO_x$ catalysts have been reported to possess a superior activity and selectivity for the oxidation of alkanes [2]. At present, the interaction of Mo, Nb, and V in these particularly active and selective catalysts is deduced from their arrangement in the ideal crystallographic structure of the as-prepared material [2]. The details of structure-activity relationships obtained from in situ investigations of these complex mixed oxides remain scarce. However, a rational design of improved catalysts will not be possible without a fundamental understanding of the relationships between the "real" structural and the catalytic properties of the mixed-oxide system under reaction conditions.

To elucidate the promotional effect of additional metal centers on the catalytic properties of mixed molybdenum oxide catalysts, suitable model systems are sought. Such systems ought to permit investigation of the influence of individual metal centers in well-defined oxide catalysts on

* Corresponding author. Fax: +49 30 8413 4405.
E-mail address: Ressler@fhi-berlin.mpg.de (T. Ressler).

0021-9517/$ – see front matter
doi:10.1016/j.jcat.2005.01.004

the structural evolution of the precursor during activation and under reaction conditions while considerably reducing the complexity of the system studied. Heteropolyoxomolybdates (HPOMs) are active catalysts for the partial oxidation of alkanes and alkenes [1–6]. They constitute suitable "real" model systems because of (i) their known structural evolution under reaction conditions, (ii) the similar onset of catalytic activity, which indicates similar active sites for alkene oxidation, and (iii) their potential to accommodate additional metal centers inside or outside of the primary Keggin ion. Moreover, HPOMs are often envisaged as ideal model systems because of their reasonably well-understood preparation procedures, which in principal make it possible to design mixed-oxide systems. However, with respect to structure-activity relationships, it has been shown that the "real" structure of the HPOM catalyst under reaction conditions does not necessarily correspond to the ideal crystallographic structure of the originally prepared Keggin-type material [7,8]. Measurement of the catalytic properties of the material must be combined with in situ structural investigations of HPOMs under reaction conditions to obtain reliable structure-activity correlations.

Recently we were able to show that migration of molybdenum centers out of the Keggin ion of $H_3[PMo_{12}O_{40}] \times 13H_2O$ onto extra-Keggin sites, resulting in a partially decomposed lacunary Keggin ion, takes place during thermal activation [9]. Conversely, thermally stable HPOMs like $Cs_3[PMo_{12}O_{40}]$, whose Keggin ions remain intact at elevated temperatures without a detectable partial decomposition, are catalytically inactive. Thus, the as-prepared and ideal Keggin ion of $H_3[PMo_{12}O_{40}] \times 13H_2O$ is only the precursor for the active catalyst, which consists of partially reduced and decomposed Keggin ions and Mo centers on extra-Keggin framework positions. A partial decomposition and migration of metal centers has previously been reported for Keggin ions with [10–14] and without addenda substituents [15–20]. In particular, with respect to the thermal activation of a vanadium-containing heteropolyoxomolybdate, $H_4[PVMo_{11}O_{40}] \times 13H_2O$, it has been proposed that substitution of vanadium for molybdenum centers destabilizes the Keggin ion, resulting in decomposition and migration of vanadium centers out of the Keggin ion [8,10–14,16,19,21,22].

Here, we present in situ X-ray diffraction (XRD) and in situ X-ray absorption spectroscopy (XAS) investigations of $H_4[PVMo_{11}O_{40}] \times 13H_2O$ during thermal treatment (i.e., activation) under reducing (propene) and catalytic (propene and oxygen) reaction conditions. In addition to a detailed structural characterization of the starting material and the catalyst obtained after thermal activation, we show that a local spectroscopy like XAS that provides a direct "image" of the structure around the vanadium centers is ideally suited to probe the local geometric structure of the active site of vanadium containing polyoxomolybdates.

2. Experimental

2.1. Preparation of $H_4[PVMo_{11}O_{40}] \times 13H_2O$

MoO_3 (18.58 g, corresponding to 11.73 mmol Mo_{11}) and V_2O_5 (1.067 g, corresponding to 11.73 mmol V) were suspended in 650 ml water in a three-necked 1000-ml flask equipped with a condenser. Commercial phosphoric acid (H_3PO_4) (∼ 82.5%) was diluted by a factor of 100, and the exact concentration was determined by titration with NaOH. Eighty-one milliliters of this solution (11.73 mmol P) was added dropwise to the boiling and stirred suspension of the metal oxides. After complete addition of the phosphoric acid, a clear amber-colored solution was obtained. The concentration of $H_4[PVMo_{11}O_{40}] \times 13H_2O$ in this solution was determined by conductometric titration to be 13.8 mmol/l. The solid product was isolated by removal of the solvent in a rotary evaporator at ∼90 °C and dried in a vacuum desiccator. X-ray fluorescence analysis afforded a Mo/V ratio of 11:1 in the as-prepared $H_4[PVMo_{11}O_{40}] \times 13H_2O$ material.

2.2. Preparation of $Cs_2H_2[PVMo_{11}O_{40}]$

Cs_2CO_3 was dissolved in water to give a solution of about 110 mmol/l. The exact concentration of the solution was determined by titration with HCl. Three hundred milliliters of the $H_4[PVMo_{11}O_{40}] \times 13H_2O$ solution (13.8 mol/l) was heated to 76 °C. An adequate amount of the Cs_2CO_3 solution (Cs/P ratio of 2:1) was diluted to 80 ml and added dropwise to the stirred solution of $H_4[PVMo_{11}O_{40}] \times 13H_2O$. To isolate the solid formed, the suspension was first reduced in volume with the use of a rotary evaporator operated at 90 °C. Subsequently, during continuous stirring the remaining slurry was dried on a Petri dish at 90 °C.

2.3. X-ray diffraction

In situ XRD experiments were performed with a STOE Theta/Theta powder diffractometer (Cu-K_α radiation, Si secondary monochromator) and a scintillation counter operated in a stepping mode. The in situ cell consisted of a PAAR XRK900 high-temperature diffraction chamber. The gas-phase composition at the cell outlet was continuously analyzed with an Omnistar quadropole mass spectrometer (Pfeiffer) in a multiple ion-monitoring mode. In situ XRD measurements were conducted at 1 bar in flowing reactants (flow rate of 100 ml/min). Gas-phase compositions of 10% propene in helium, or 10% propene and 10% oxygen in helium were used. XRD patterns were measured every 25 K in the temperature range from 315 to 773 K, resulting in an effective heating rate of 1.3 K/min. A description of the procedure used can be found in Ref. [23]. Ex situ XRD measurements were performed on a STOE STADI P diffractometer (Cu-K_{α_1}; Ge primary monochromator) in a range of 5° to 100° in 2θ with a step width of 0.01° and a measuring time

of 10 s/step. Structural refinements to the experimental diffraction patterns were performed with the software TOPAS v 2.1 (Bruker AXS). Structural data used in the XRD and XAS analyses were taken from the Inorganic Crystal Structure Database (ICSD).

2.4. X-ray absorption spectroscopy

In situ transmission XAS experiments were performed at the Mo K edge (19.999 keV) at beamline X1 at the Hamburg Synchrotron Radiation Laboratory (HASYLAB), with the use of a Si 311 double crystal monochromator. The storage ring was operated at 4.4 GeV with injection currents of 150 mA. The in situ experiments were conducted in a flow reactor [23,24] at 1 bar in flowing reactants (flow rate of 30 ml/min, temperature range from 300 to 773 K at 5 K/min, subsequently held at 773 K). The gas-phase composition at the cell outlet was continuously analyzed with a mass spectrometer in a multiple ion-monitoring mode (Omnistar from Pfeiffer). The heteropolyoxomolybdates were mixed with boron nitride and pressed with a force of 1 ton into a 5-mm-diameter pellet, resulting in an edge jump at the Mo K-edge of $\Delta\mu_x \sim 1.5$ (~ 7 mg HPOM and ~ 30 mg BN).

Because of the low concentration of vanadium in a heavily absorbing matrix (Mo and Cs atoms), ex situ XAS measurements at the V K-edge (5.465 keV) were conducted at the High Brilliance X-ray Spectroscopy Beamline ID26 at the European Synchrotron Radiation Facility (ESRF). $Mo_x[PVMo_{11-x}O_{40}]$ and $Cs_2Mo_x[PVMo_{11-x}O_{40}]$ were prepared from $H_4[PVMo_{11}O_{40}] \times 13H_2O$ and $Cs_2H_2[PVMo_{11}O_{40}]$, respectively, in the in situ XRD setup according to the procedure described above and sealed in an argon atmosphere. The samples were mixed with cellulose in a ratio of 1:10, placed on a sample holder, and measured at 50 K. Spectra were collected in the fluorescence mode with a measuring time of about 7 min.

X-ray absorption fine structure (XAFS) analysis was performed with the software package WinXAS v3.1 [25] according to recommended procedures from the literature [26]. We carried out background subtraction and normalization by fitting linear polynomials to the pre-edge and the post-edge regions of an absorption spectrum, respectively. The extended X-ray absorption fine structure (EXAFS) $\chi(k)$ was extracted with the use of cubic splines to obtain a smooth atomic background, $\mu_0(k)$. We calculated the pseudo-radial distribution function $FT(\chi(k)k^3)$ by Fourier transforming the k^3-weighted experimental $\chi(k)$ function, multiplied by a Bessel window, into the R space. EXAFS data analysis was performed with the use of theoretical backscattering phases and amplitudes calculated with the ab initio multiple-scattering code FEFF7 [27]. Single scattering and multiple scattering paths in the Keggin ion model structure were calculated up to 6.0 Å with a lower limit of 2.0% in amplitude with respect to the strongest backscattering path. EXAFS refinements were performed in R space simultaneously to magnitude and the imaginary part of a Fourier-transformed k^3-weighted and k^1-weighted experimental $\chi(k)$, with use of the standard EXAFS formula [28]. Structural parameters that are determined by a least-squares EXAFS refinement of a Keggin model structure to the experimental spectra are (i) one overall E_0 shift, (ii) Debye–Waller factors for single-scattering paths, (iii) distances of single-scattering paths, and (iv) one-third cumulant for the Mo–O distances in the first coordination shell and one-third cumulant for all remaining scattering paths. Coordination numbers (CNs) and S_0^2 were kept invariant in the refinement.

3. Results

3.1. Characterization of $H_4[PVMo_{11}O_{40}] \times 13H_2O$

The ex situ X-ray diffraction pattern of as-prepared $H_4[PVMo_{11}O_{40}] \times 13H_2O$ is depicted in Fig. 1. The simulated pattern shown in Fig. 1 was obtained from a refinement of a $H_3[PMo_{12}O_{40}] \times 13H_2O$ model structure to the experimental pattern ($H_3[PMo_{12}O_{40}] \times 13H_2O$, P-1, [ICSD 31128, $a = 14.10$ Å, $b = 14.13$ Å, $c = 13.55$ Å, $\alpha = 112.1°$, $\beta = 109.8°$, $\gamma = 60.7°$]; $H_4[PVMo_{11}O_{40}] \times 13H_2O$, P-1, [$a = 14.08$ Å, $b = 14.11$ Å, $c = 13.52$ Å, $\alpha = 112.1°$, $\beta = 109.6°$, $\gamma = 60.9°$]; atomic coordinates were kept invariant in the refinement). A schematic representation of the structure of $H_4[PVMo_{11}O_{40}] \times 13H_2O$ is shown in the inset of Fig. 1. The evolution of the relative sample weight (TG) during thermal treatment of $H_4[PVMo_{11}O_{40}] \times 13H_2O$ in oxygen has previously been described [21]. A weight loss detected in the temperature range from 300 to 523 K corresponds to the loss of crystal water from as-prepared $H_4[PVMo_{11}O_{40}] \times 13H_2O$. A further weight loss, a second peak in the water signal, and an endothermic DSC signal at 573 K correspond to the loss of so-called structural water of $H_4[PVMo_{11}O_{40}] \times 13H_2O$. As will be discussed later, this temperature coincides with the onset of catalytic activity. UV–vis spectra of $H_4[PVMo_{11}O_{40}] \times 13H_2O$ measured in solution exhibited an additional band compared with $H_3[PMo_{12}O_{40}] \times 13H_2O$, indicating the incorporation of vanadium into the Keggin ion.

Fig. 2 shows two experimental XAFS $\chi(k)k^3$ of $H_4[PVMo_{11}O_{40}] \times 13H_2O$ measured at the Mo and V K-edges at 300 and 50 K, respectively. The Mo K-edge spectrum was measured in about 4.5 min. The signal-to-noise ratio up to 14 $Å^{-1}$ at the V K-edge and 15 $Å^{-1}$ at the Mo K-edge is certainly sufficient for the XAFS analysis described below. The experimental and theoretical Mo K-edge $FT(\chi(k)k^3)$ of $H_4[PVMo_{11}O_{40}] \times 13H_2O$ and $H_3[PMo_{12}O_{40}] \times 13H_2O$ are depicted in Fig. 3, together with a schematic representation of the Keggin ion. The theoretical $FT(\chi(k)k^3)$ were obtained from a refinement of a Keggin model structure to the Mo K-edge data of $H_4[PVMo_{11}O_{40}] \times 13H_2O$ and $H_3[PMo_{12}O_{40}] \times 13H_2O$. The local structure parameters obtained correspond to those

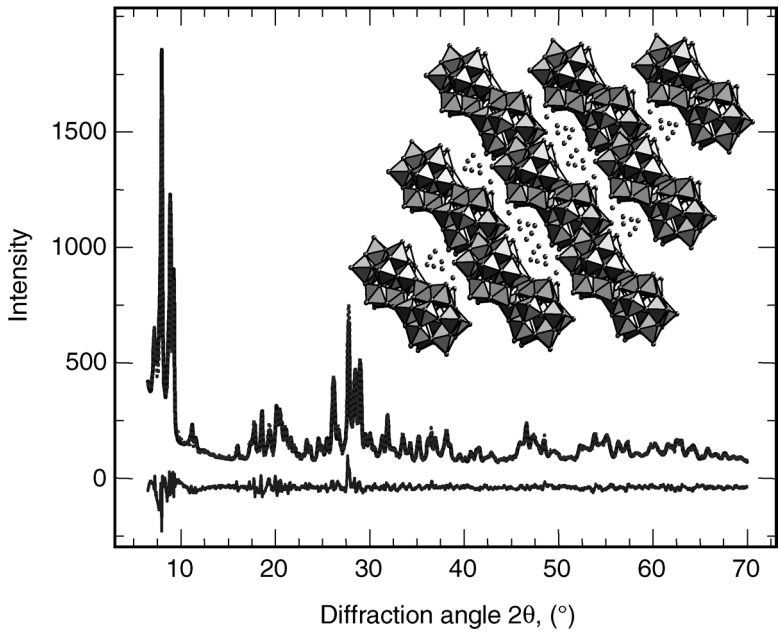

Fig. 1. Experimental (dotted) and simulated (solid) X-ray diffraction pattern of as-prepared $H_4[PVMo_{11}O_{40}] \times 13H_2O$ (P-1, $a = 14.08$ Å, $b = 14.11$ Å, $c = 13.52$ Å, $\alpha = 112.1°$, $\beta = 109.6°$, $\gamma = 60.9°$). The inset shows a schematic structural representation of $H_4[PVMo_{11}O_{40}] \times 13H_2O$.

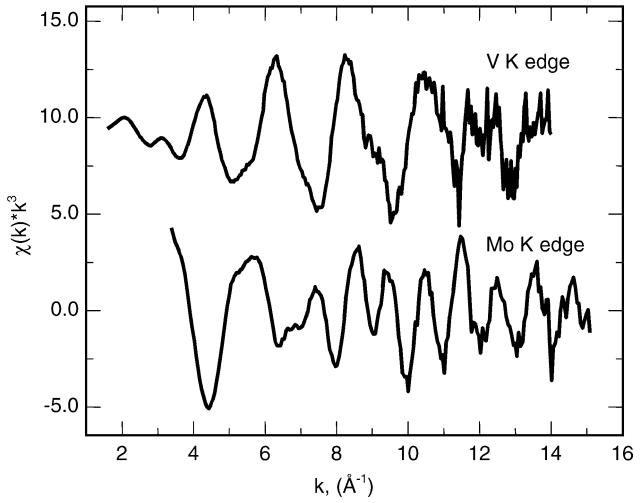

Fig. 2. Experimental XAFS $\chi(k)k^3$ of $H_4[PVMo_{11}O_{40}] \times 13H_2O$ measured at the V K-edge (50 K) and at the Mo K-edge (room temperature, 4.5 min/spectrum).

reported in the literature [9], with insignificant deviations between $H_4[PVMo_{11}O_{40}] \times 13H_2O$ and $H_3[PMo_{12}O_{40}] \times 13H_2O$. The experimental and theoretical V K-edge $FT(\chi(k)k^3)$ of $H_4[PVMo_{11}O_{40}] \times 13H_2O$ is depicted in Fig. 4I. The theoretical $FT(\chi(k)k^3)$ was obtained from a refinement of a Keggin model structure to the V K-edge data of $H_4[PVMo_{11}O_{40}] \times 13H_2O$. The local structure parameters obtained are listed in Table 1. The local structure around a V center in the Keggin ion is shown in Fig. 5.

3.2. *Thermal treatment of $H_4[PVMo_{11}O_{40}] \times 13H_2O$ in propene*

The evolution of XRD patterns measured during thermal treatment of $H_4[PVMo_{11}O_{40}] \times 13H_2O$ in 10% propene in the temperature range from 323 to 723 K resembles that presented in the literature for the thermal treatment of $H_3[PMo_{12}O_{40}] \times 13H_2O$ [9]. Under these conditions a single-phase cubic HPOM is obtained at 773 K without further decomposition and reduction to MoO_2. The background-corrected and normalized XRD pattern of the cubic HPOM at 300 K in comparison with that obtained from a thermal treatment of $H_3[PMo_{12}O_{40}] \times 13H_2O$ is depicted in Fig. 6. Except for the strongest peak at about 27°, a very good agreement between the intensity ratios of the peaks in the two experimental patterns can be seen. The simulated diffraction pattern shown in Fig. 7A was obtained from a refinement of the structure of cubic $Mo_x[PVMo_{11-x}O_{40}]$ to the experimental pattern. The structural data determined for $Mo_x[PVMo_{11-x}O_{40}]$ are listed in Table 2. A schematic representation of cubic $Mo_x[PVMo_{11-x}O_{40}]$ is depicted in Fig. 7B.

The evolution of the Mo K-near-edge spectra of $H_4[PVMo_{11}O_{40}] \times 13H_2O$ resembles that of $H_3[PMo_{12}O_{40}] \times 13H_2O$ as reported in Ref. [9]. Refinement of a Keggin model structure to the experimental Mo K-edge $FT(\chi(k)k^3)$ of $Cs_2H_2[PVMo_{11}O_{40}]$ and $Cs_2H[PMo_{12}O_{40}]$ during thermal treatment in 10% propene was performed to elucidate the evolution of the average local structure around a Mo center. For comparison of the structural evolution of V-containing and V-free Keggin ion, the Cs salts of $H_4[PVMo_{11}O_{40}] \times 13H_2O$ and $H_3[PMo_{12}O_{40}] \times 13H_2O$ were chosen because of their superior thermal stability against decomposition to MoO_3. The presence of a major amount of MoO_3 would render a reliable determination of the average local Keggin structure under reaction conditions more difficult. The evolution of selected Mo–O and Mo–Mo distances in the average local structure around a Mo

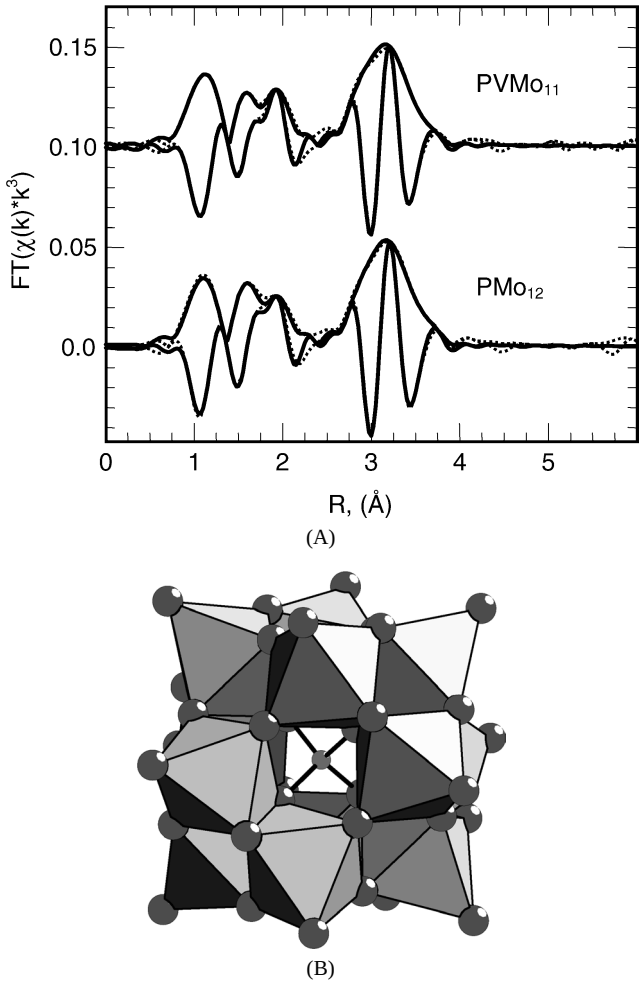

Fig. 3. (A) Experimental (dotted) and theoretical (solid) $FT(\chi(k)k^3)$ of the Mo K-edge spectra of $H_4[PVMo_{11}O_{40}] \times 13H_2O$ ($PVMo_{11}$) and $H_3[PMo_{12}O_{40}] \times 13H_2O$ (PMo_{12}) together with (B) a schematic representation of the Keggin ion.

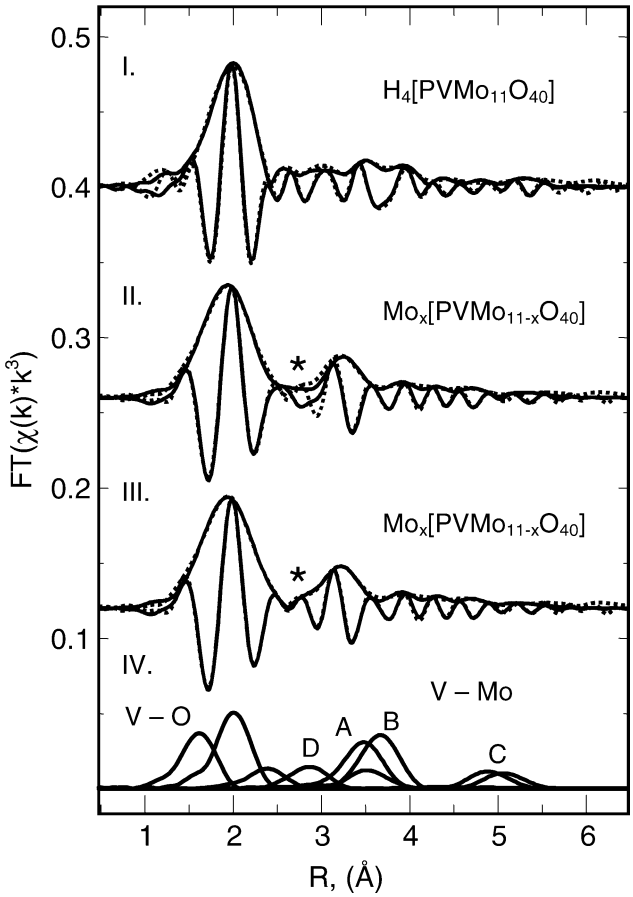

Fig. 4. Experimental (dotted) and theoretical (solid, Table 1) $FT(\chi(k)k^3)$ of the V K-edge spectra of (I) $H_4[PVMo_{11}O_{40}] \times 13H_2O$, (II) $Mo_x[PVMo_{11-x}O_{40}]$ without taking shell D into account, (III) $Mo_x[PVMo_{11-x}O_{40}]$ taking shell D into account, and (IV) single scattering shells in the local structure around the V center in the Keggin ion (schematic representation in Fig. 5). The $FT(\chi(k)k^3)$ have been arbitrarily phase corrected by a shift of 0.4 Å.

center in $Cs_2H_2[PVMo_{11}O_{40}]$ and $Cs_2H[PMo_{12}O_{40}]$ during thermal treatment in 10% propene is depicted in Fig. 8. At temperatures above 573 K a significant increase in the selected Mo–O and Mo–Mo distances can be seen. For the Mo–Mo distances chosen, the structural transformation appears to be finished at ∼ 700 K, resulting in a stable phase upon further heating.

Table 1
Structural parameters (type of pairs and number (N) of nearest neighbors at distance R) obtained from a refinement of a Keggin ion model structure (based on ICSD 209, Table 2) to the experimental XAFS functions $\chi(k)$ of $H_4[PVMo_{11}O_{40}] \times 13H_2O$ (Fig. 4) and cubic $Mo_x[PVMo_{11-x}O_{40}]$ (Fig. 4) at the V K-edge ($N_{ind} = 35$, $N_{free} = 20$, 12 single scattering paths and 7 multiple scattering paths, $E_0 = -7.3$ eV)

	$H_4[PVMo_{11}O_{40}] \times 13H_2O$		$H_4[PVMo_{11}O_{40}] \times 13H_2O$			$Mo_x[PVMo_{11-x}O_{40}]$		
Type	N	R (Å)	N	R (Å)	σ^2 (Å^2)	N	R (Å)	σ^2 (Å^2)
V–O	1	1.71	1	1.62	0.0038	1	1.64	0.0048
V–O	2	1.91	2	1.97	0.0040	2	2.00	0.0054
V–O	2	1.92	2	1.97	0.0040	2	2.00	0.0054
V–O	1	2.46	1	2.46	0.0042	1	2.44	0.0038
V–Mo	2	3.42	2	3.33	0.0063	2	3.44	0.0051
V–P	1	3.57	1	3.50	0.001	1	3.52	0.001
V–Mo	2	3.72	2	3.68	0.0024	2	3.66	0.0039
V–Mo	2	4.89	2	4.86	0.0086	2	4.92	0.0066
V–Mo	2	5.02	2	5.04	0.0086	2	5.08	0.0066
V–Mo			–	–	–	0.6	2.84	0.0051

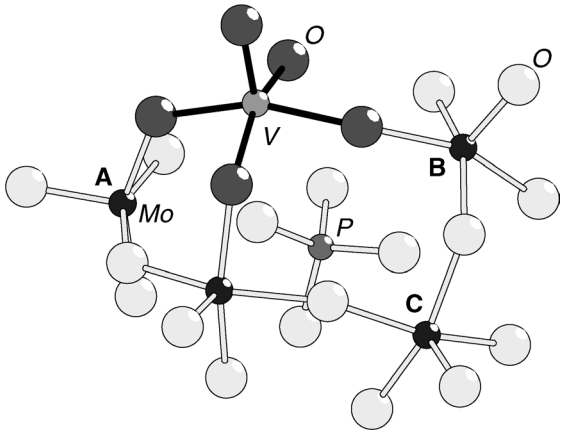

Fig. 5. Schematic representation of the local structure around the V center in the Keggin ion of $H_4[PVMo_{11}O_{40}] \times 13H_2O$. The neighboring Mo centers are indicated (A, V–Mo at 3.4 Å; B, V–Mo at 3.8 Å; C, V–Mo at 5 Å).

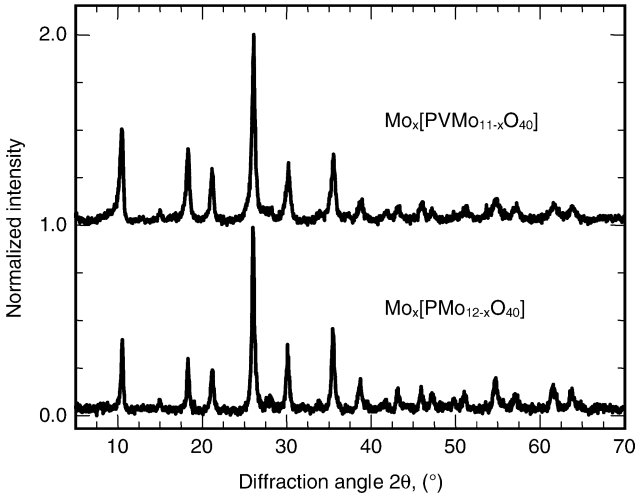

Fig. 6. Comparison of the experimental XRD patterns of cubic $Mo_x[PVMo_{11-x}O_{40}]$ and $Mo_x[PMo_{12-x}O_{40}]$ obtained from thermal treatment of $H_4[PVMo_{11}O_{40}] \times 13H_2O$ and $H_4[PMo_{12}O_{40}] \times 13H_2O$, respectively, in 10% propene in He.

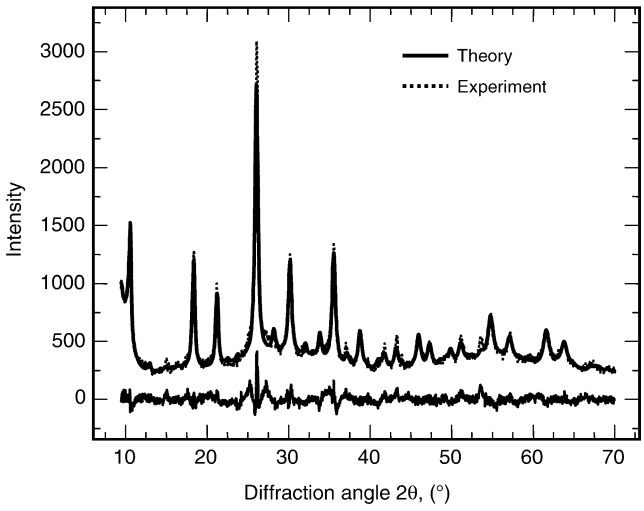

(A)

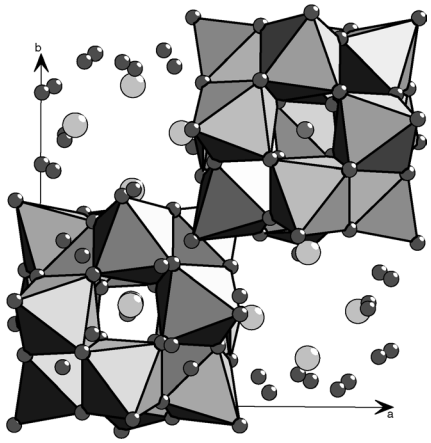

(B)

Fig. 7. (A) Experimental and simulated XRD patterns of cubic $Mo_x[PVMo_{11-x}O_{40}]$ (Table 2) obtained from thermal treatment of $H_4[PVMo_{11}O_{40}] \times 13H_2O$ in 10% propene in He from 300 to 773 K. (B) Schematic structural representation of the cubic $Mo_x[PVMo_{11-x}O_{40}]$ phase.

Table 2
Atom coordinates in the unit cell of $Mo_x[PVMo_{11-x}O_{40}]$ obtained from a refinement of a structural model based on $K_2H[PMo_{12}O_{40}] \times H_2O$ (ICSD 209, Pn-3mZ, $a = 11.6$ Å], with K and H_2O omitted) with a molybdenum center (Mo2) on an extra-Keggin framework position (Pn-3mZ, $a = 11.861$ Å). Atom coordinates were kept invariant in the refinement except for the coordinates of the extra-Keggin Mo center

Site	x	y	z	Occ
Mo1	0.4670	0.4670	0.2587	0.94 (2)
O1	0.6528	0.6528	0.0060	1
O2	0.0689	0.0689	0.7670	1
O3	0.1233	0.1233	0.5398	1
O4	0.3273	0.3273	0.3273	1
P1	0.2500	0.2500	0.2500	1
Mo2	0.403 (3)	0.764 (3)	0.764 (3)	0.15 (1)

V K-near-edge spectra for $H_4[PVMo_{11}O_{40}] \times 13H_2O$, cubic $Mo_x[PVMo_{11-x}O_{40}]$, and various vanadium oxide references (V_2O_3, VO_2, V_2O_5) are depicted in Fig. 9. The reduction in the height of the characteristic V K-pre-edge peak at 5.47 keV indicates a reduction of mostly V^{5+} in $H_4[PVMo_{11}O_{40}] \times 13H_2O$ to mostly V^{4+} in $Mo_x[PVMo_{11-x}O_{40}]$. Fig. 4II shows the $FT(\chi(k)k^3)$ of cubic $Mo_x[PVMo_{11-x}O_{40}]$ together with a theoretical refinement of the local structure around a V center substituting for Mo in the Keggin ion. The structural parameters determined are listed in Table 1. The refinement results in a good agreement in the range between 1.5 and 2.5 Å and between 3.5 and 5.0 Å. However, a considerable deviation between experimental data and simulation can be observed at about 2.9 Å. Only after the simulation was extended by an additional Mo–Mo shell at about 2.9 Å (D in Fig. 4IV) could a satisfying agreement between theory and simulation over the entire data range be obtained (Fig. 4III). A comparison between the V K-edge $FT(\chi(k)k^3)$ of $H_4[PVMo_{11}O_{40}] \times 13H_2O$ and cubic $Mo_x[PVMo_{11-x}O_{40}]$ is depicted in Fig. 10. Evidently, the two $FT(\chi(k)k^3)$ agree reasonably well at around

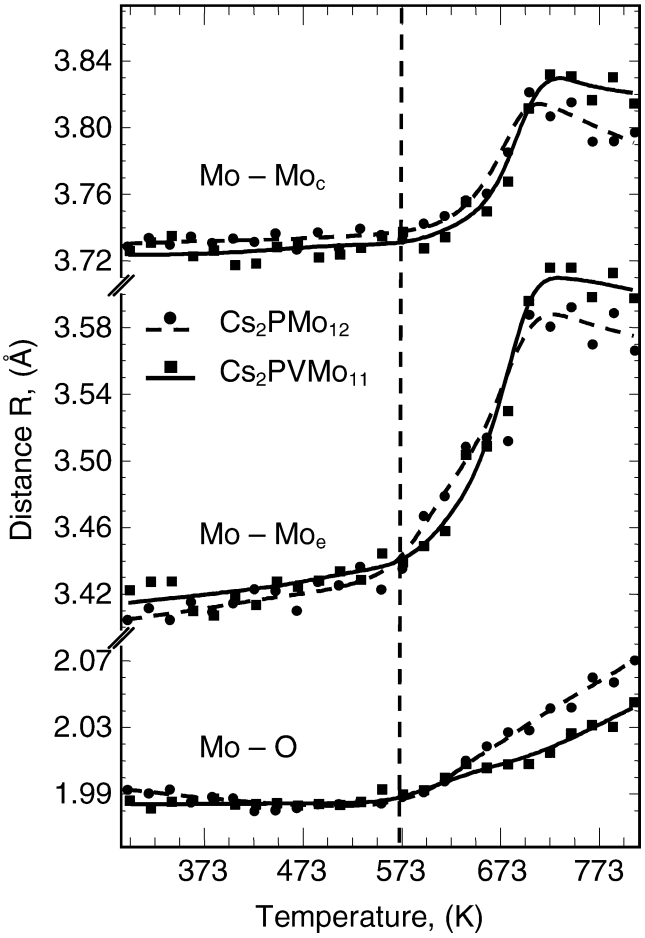

Fig. 8. Evolution of representative Mo–O and Mo–Mo distances in the average local structure around a Mo center in $Cs_2H_2[PVMo_{11}O_{40}]$ and $Cs_2H[PMo_{12}O_{40}]$ in 10% propene in He. The dashed line indicates the onset of catalytic activity.

2.0 Å and in the range from 3.2 to 6.0 Å, whereas considerable deviations can be seen between 2.5 and 3.2 Å.

3.3. Thermal activation of $H_4[PVMo_{11}O_{40}] \times 13H_2O$ in propene and oxygen

From Mo K-edge XANES spectra measured during thermal treatment of $Cs_2H_2[PVMo_{11}O_{40}]$ and $Cs_2H[PMo_{12}O_{40}]$ in 10% propene and 10% oxygen in He, an average Mo valence was determined according to the procedure reported in Ref. [29]. Fig. 11 shows the evolution of the Mo average valence together with the normalized propene conversion. $Cs_2H_2[PVMo_{11}O_{40}]$ and $Cs_2H[PMo_{12}O_{40}]$ exhibit the same onset of catalytic activity at $\sim$ 573 K, which roughly correlates with a partial reduction of the molybdenum in the Keggin ions. Compared with $Cs_2H[PMo_{12}O_{40}]$, the Mo centers in $Cs_2H_2[PVMo_{11}O_{40}]$ appear to be reduced at slightly lower temperatures. At temperatures above 700 K a decrease in the catalytic activity can be seen that coincides with an oxidation of the molybdenum and a possible decomposition of the HPOM. A Keggin model structure was refined to the experimental Mo K-edge $FT(\chi(k)k^3)$ of

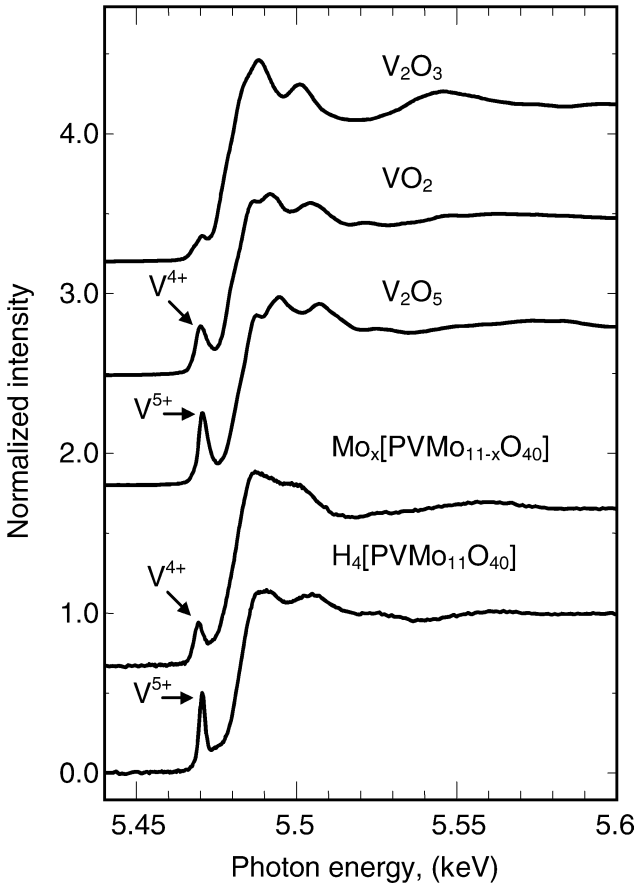

Fig. 9. V K-near-edge spectra of $H_4[PVMo_{11}O_{40}] \times 13H_2O$, $Mo_x[PVMo_{11-x}O_{40}]$, and various vanadium oxide references (V_2O_3, VO_2, V_2O_5).

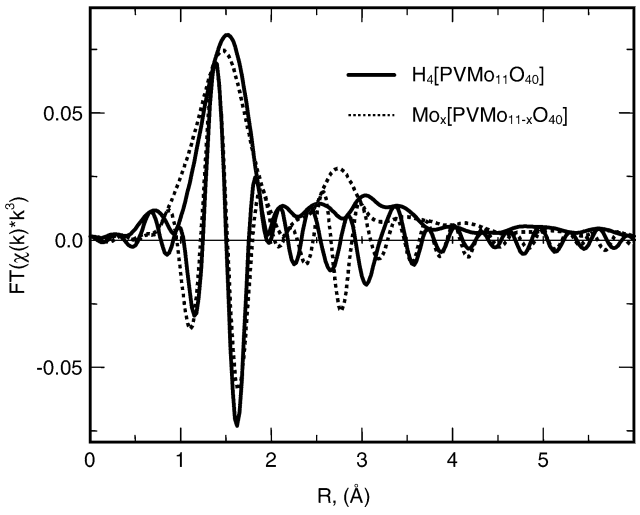

Fig. 10. Experimental $FT(\chi(k)k^3)$ of the V K-edge spectra of $H_4[PVMo_{11}O_{40}] \times 13H_2O$ ($PVMo_{11}$, solid) and $Mo_x[PVMo_{11-x}O_{40}]$ (dotted).

$Cs_2H_2[PVMo_{11}O_{40}]$ and $Cs_2H[PMo_{12}O_{40}]$ measured during thermal treatment in 10% propene and 10% oxygen to determine the structural evolution during activation. Characteristic changes in selected Mo–O and Mo–Mo distances

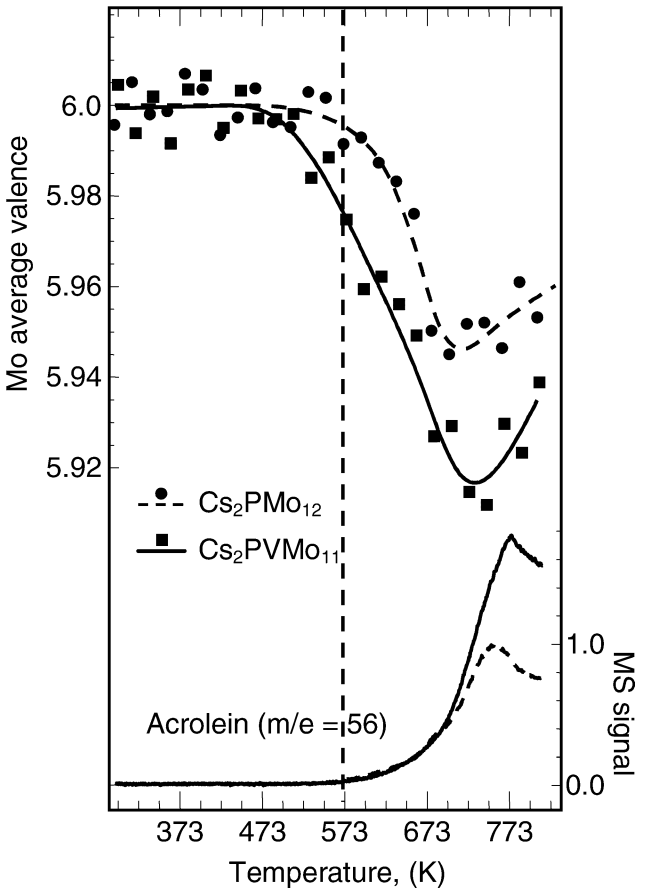

Fig. 11. Evolution of average Mo valence obtained from Mo K-edge XANES spectra measured during thermal treatment of $Cs_2H_2[PVMo_{11}O_{40}]$ and $Cs_2H[PMo_{12}O_{40}]$ in 10% propene and 10% oxygen in He together with the normalized ion current of acrolein ($m/e = 56$).

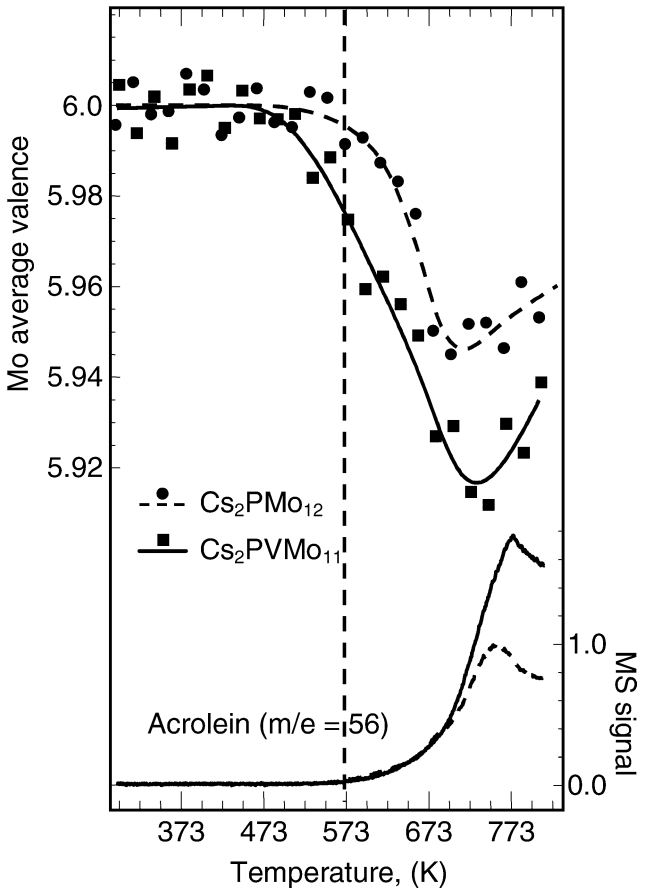

Fig. 12. Evolution of representative Mo–O and Mo–Mo distances in the average local structure around a Mo center in $Cs_2H_2[PVMo_{11}O_{40}]$ and $Cs_2H[PMo_{12}O_{40}]$ in 10% propene and 10% oxygen in He together with the normalized ion current of acrolein ($m/e = 56$).

during thermal treatment in propene and oxygen are shown in Fig. 12 together with the propene conversion. The onset of catalytic activity coincides with an increase in the Mo–O and Mo–Mo distance in both $Cs_2H_2[PVMo_{11}O_{40}]$ and $Cs_2H[PMo_{12}O_{40}]$, and the amplitudes of the changes detected in the two materials are very similar.

3.4. Stability and solid-state dynamics of $Mo_x[PVMo_{11-x}O_{40}]$ in propene and oxygen

We investigated the stability and catalytic activity of cubic $Mo_x[PVMo_{11-x}O_{40}]$ prepared from $H_4[PVMo_{11}O_{40}] \times 13H_2O$ by subjecting the material to a temperature-programmed reaction (TPR) experiment in 10% propene and 10% oxygen in the temperature range from 300 to 773 K in the in situ XRD setup. The evolution of XRD patterns of $Mo_x[PVMo_{11-x}O_{40}]$ measured during the thermal treatment is depicted in Fig. 13A. $Mo_x[PVMo_{11-x}O_{40}]$ exhibits a remarkable stability up to temperatures of about 673 K. At temperatures above 673 K slight changes to the pattern of $Mo_x[PVMo_{11-x}O_{40}]$ can be observed together with the occurrence of additional peaks. The evolution of the ion current of acrolein ($m/e = 56$) during TPR of $Mo_x[PVMo_{11-x}O_{40}]$ in propene and oxygen is shown in Fig. 13B. Evidently, the onset of catalytic activity at ~ 550 K does not correlate with significant changes in the long-range structure of $Mo_x[PVMo_{11-x}O_{40}]$.

Changes in the average local structure around the Mo centers in $Mo_x[PVMo_{11-x}O_{40}]$ during TPR of 10% propene and 10% oxygen between 300 and 723 K were determined by Mo K-edge XAS measurements. Structural parameters were obtained from a refinement of a Keggin structure to the experimental spectra measured. The evolution of selected Mo–O distances in $Mo_x[PVMo_{11-x}O_{40}]$ during TPR is depicted in Fig. 14. The ion current of acrolein ($m/e = 56$) measured during TPR of $Mo_x[PVMo_{11-x}O_{40}]$ exhibits an onset of catalytic activity at about 573 K, accompanied by a characteristic decrease in the Mo–O distances shown. Subsequently, the temperature was held at 723 K and the gas phase was switched between a reducing (propene) and an oxidizing (propene and oxygen) atmosphere. It can be seen that the local Mo structure can be reversibly changed from a reduced to an oxidized state of the catalytically active phase (Fig. 14).

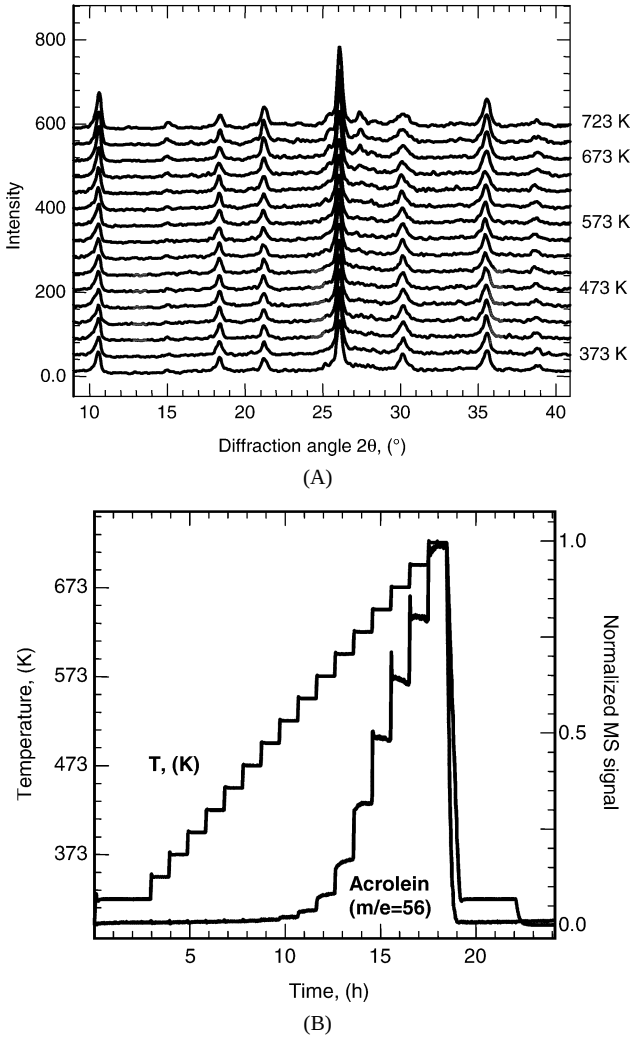

Fig. 13. (A) Evolution of XRD patterns of $Mo_x[PVMo_{11-x}O_{40}]$ during temperature programmed reaction of 10% propene and 10% oxygen in He in the range from 300 to 773 K. (B) Evolution of the normalized ion current of acrolein ($m/e = 56$) with reaction temperature.

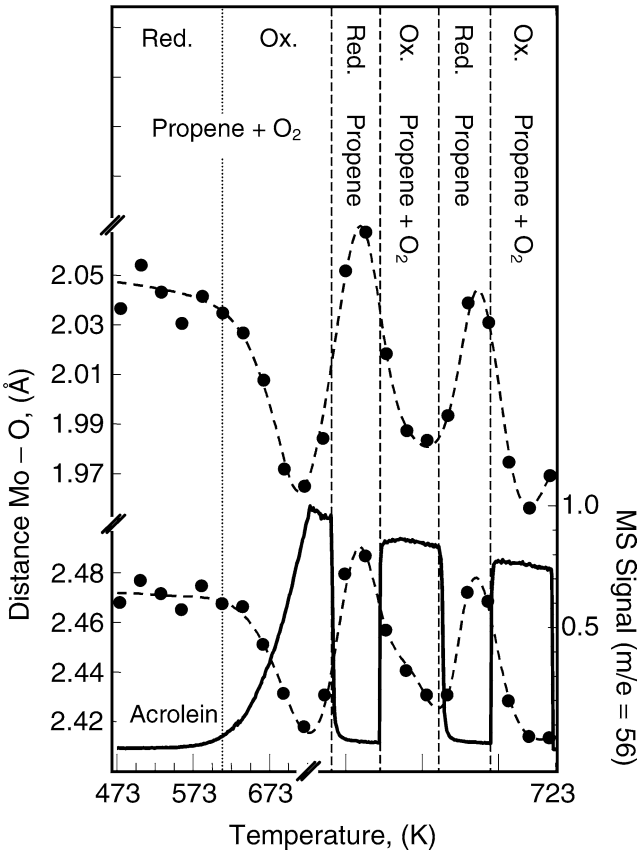

Fig. 14. Evolution of selected Mo–O distances in the average local structure around a Mo center in $Mo_x[PVMo_{11-x}O_{40}]$ together with the normalized ion current of acrolein ($m/e = 56$) during temperature programmed reaction of 10% propene and 10% oxygen in He from 373 to 673 K followed by isothermal switching experiments between reducing (propene) and oxidizing (propene and oxygen) atmosphere. The reduced (Red.) or oxidized (Ox.) state of the active site depending on the reaction conditions is indicated.

4. Discussion

4.1. Characterization of $H_4[PVMo_{11}O_{40}] \times 13H_2O$

To elucidate the evolution of the local structure around a V center in a mixed molybdenum oxide under reaction conditions, a heteropolyoxomolybdate $H_4[PVMo_{11}O_{40}] \times 13H_2O$ with V centers substituting for Mo in the Keggin ion was prepared. Because some of the debate in the literature arises from the difficulties in comparing the various starting materials used, a rather detailed account of the preparation procedure employed and the structural characterization is provided. The long-range order structure of the as-prepared $H_4[PVMo_{11}O_{40}] \times 13H_2O$ is similar to that of $H_3[PMo_{12}O_{40}] \times 13H_2O$ (Fig. 1), indicating that vanadium is indeed located in the Keggin ion. If V were situated on extra-Keggin framework positions, the formation of the characteristic triclinic "13-hydrate" structure would not be expected. A vanadyl species located outside the Keggin ion will most likely result in the formation of a HPOM possessing a higher crystallographic symmetry (e.g., a cubic phase similar to the Cs salts of $H_3[PMo_{12}O_{40}] \times 13H_2O$). Moreover, the local structure around the V centers in $H_4[PVMo_{11}O_{40}] \times 13H_2O$ as determined by V K-edge XAS (Fig. 4, Table 1) is in good agreement with a V site in the Keggin ion for the majority of vanadium in the material prepared (Fig. 5). The local average structure around the Mo centers in $H_4[PVMo_{11}O_{40}] \times 13H_2O$ is hardly affected by the presence of V in the Keggin ion (Fig. 3). The thermal stability of $H_4[PVMo_{11}O_{40}] \times 13H_2O$ resembles the typical behavior of heteropolyoxomolybdates [21] during thermal treatment with a loss of crystal water at temperatures below 573 K and a loss of structural water above 573 K, accompanied by partial decomposition of the Keggin ions. The endothermic loss of structural water at $\sim$ 573 K coincides with the onset of catalytic activity and characteristic structural changes during thermal activation of $H_4[PVMo_{11}O_{40}] \times 13H_2O$ in propene and in propene and oxygen (Figs. 11 and 12).

4.2. Thermal treatment of $H_4[PVMo_{11}O_{40}] \times 13H_2O$ in propene

Previously we reported the formation of a cubic HPOM from $H_3[PMo_{12}O_{40}] \times 13H_2O$ by thermal treatment in propene in the temperature range from 300 to 773 K [9]. The cubic HPOM (i.e., $Mo_x[PMo_{12-x}O_{40}]$) obtained is characterized by Mo centers on extra-Keggin framework positions (Fig. 7B) and a superior catalytic activity in propene oxidation compared with the as-prepared HPOM. Furthermore, the onset temperature for the formation of the cubic HPOM coincided with the onset of catalytic activity at ∼ 573 K. Evidently, from the thermal treatment of $H_4[PVMo_{11}O_{40}] \times 13H_2O$ in propene a similar cubic HPOM (i.e., $Mo_x[PVMo_{11-x}O_{40}]$) can be obtained that exhibits a long-range ordered structure comparable to that of the cubic HPOM obtained from $H_3[PMo_{12}O_{40}] \times 13H_2O$ (Figs. 6, 7, Table 2 [9]). If during treatment of $H_4[PVMo_{11}O_{40}] \times 13H_2O$, vanadium had migrated to extra-Keggin framework positions instead of Mo, such a good agreement of the XRD patterns of the two cubic phases would not be expected. In total, a site occupancy of ∼ 0.15 (Table 2), together with 12 suitable extra-Keggin sites and two Keggin ions per unit cell, amounts to about one extra-Keggin molybdenum center per Keggin ion (1.8 per two Keggin ions). Conversely, with V present on an extra-Keggin framework position, a site occupancy of ∼ 0.3 would amount to about two vanadium centers per Keggin ions, which exceeds the number of V centers available in $H_4[PVMo_{11}O_{40}] \times 13H_2O$. In addition to the structural similarity of the cubic phases obtained from thermal treatment of $H_3[PMo_{12}O_{40}] \times 13H_2O$ and $H_4[PVMo_{11}O_{40}] \times 13H_2O$, the average local structure around the Mo centers in a V-containing Keggin ion and a V-free Keggin ion evolves similarly during treatment in propene (Fig. 8). The onset of the structural changes in the Keggin ion at ∼ 573 K is again correlated with the characteristic weakening of the Mo–O bond detectable in various molybdenum oxides [29,30], which in turn coincides with the onset of catalytic activity. Neither seems to be effected by the presence of V in the Keggin ions of $H_4[PVMo_{11}O_{40}] \times 13H_2O$.

The good agreement between the experimental XRD patterns of the two cubic phases in Fig. 6 and the corresponding structural data given in Table 2 is, however, only indirect evidence for the V centers residing in the lacunary Keggin ions of the cubic HPOM obtained from $H_4[PVMo_{11}O_{40}] \times 13H_2O$. Therefore, element-specific X-ray absorption spectroscopy was used to determine the average valence and the local structure around the V center. From an analysis of the V *K*-near-edge spectra [31] it is evident that the V is present as V^{5+} in the Keggin ion of as-prepared $H_4[PVMo_{11}O_{40}] \times 13H_2O$ and is reduced from V^{5+} to V^{4+} during thermal activation and formation of the cubic HPOM [32]. The detailed local structure of the vanadium in cubic $Mo_x[PVMo_{11-x}O_{40}]$ was obtained from an analysis of the V *K*-edge EXAFS spectra (Fig. 4). The experimental $FT(\chi(k)k^3)$ of cubic $Mo_x[PVMo_{11-x}O_{40}]$ obtained from $H_4[PVMo_{11}O_{40}] \times 13H_2O$ is in good agreement with the theoretical XAFS calculation, assuming that V is still situated on a Mo site in the Keggin ion (Fig. 4II). Both the V–O and V–Mo distances and the corresponding Debye–Waller factors deviate only slightly from those of as-prepared $H_4[PVMo_{11}O_{40}] \times 13H_2O$ (Table 1). These deviations result mostly from the local structural changes caused by the reduction of the vanadium and the partial decomposition of the Keggin ion. The close relationship of the medium-range order around the V center in $H_4[PVMo_{11}O_{40}] \times 13H_2O$ and $Mo_x[PVMo_{11-x}O_{40}]$ is also evident from the very similar amplitude and imaginary part in their corresponding $FT(\chi(k)k^3)$ above 3.5 Å, which includes the characteristic V–Mo distances inside the Keggin ion.

With the otherwise very good agreement between theory and experiment, the considerable deviation at about 2.8 Å in the $FT(\chi(k)k^3)$ of $Mo_x[PVMo_{11-x}O_{40}]$ (Fig. 4II) and in the comparison between $H_4[PVMo_{11}O_{40}] \times 13H_2O$ and $Mo_x[PVMo_{11-x}O_{40}]$ (Fig. 10) is particularly prominent. As can be seen from Fig. 4III, we can significantly improve the agreement between theory and experiment by considering an additional Mo center with a V–Mo distance of ∼ 2.8 Å (D in Fig. 4IV, Table 1). This distance corresponds very well with the distance from a V center in a Keggin ion to a Mo center on an extra-Keggin position, according to the structural data determined by the XRD refinement to the pattern of $Mo_x[PVMo_{11-x}O_{40}]$ (Fig. 7A, Table 2) [9,17,18]. A schematic representation of the local structure around the V center in activated cubic $Mo_x[PVMo_{11-x}O_{40}]$ is depicted in Fig. 15. The structure of the partial Keggin ion shown corresponds to the data given in Table 2, and the V–O and V–Mo distances indicated are obtained from a structure refinement

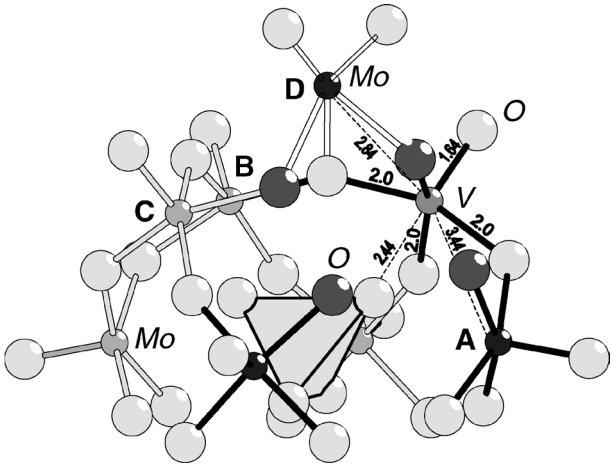

Fig. 15. Schematic representation of the local structure around the V center in activated cubic $Mo_x[PVMo_{11-x}O_{40}]$. The upper half of the Keggin ion shown corresponds to the structural data given in Table 2. V–O and V–Mo distances indicated are obtained from a structure refinement to the V *K*-edge data (Table 1). A–D indicate V–Mo distances corresponding to the $FT(\chi(k)k^3)$ in Fig. 4IV.

to the V K-edge data (Table 1). A–D indicate V–Mo distances corresponding to the $FT(\chi(k)k^3)$ in Fig. 4IV.

A Mo center at a distance of 2.8 Å from the V center in the Keggin ion confirms the migration of metal centers out of the Keggin ion onto extra-Keggin framework positions during thermal treatment of $H_4[PVMo_{11}O_{40}] \times 13H_2O$ in propene. Together with the good agreement between the experimental data and the calculated EXAFS function based on a structural model with V in the Keggin ion, this clearly shows that indeed Mo migrates onto an extra-Keggin site. A V–Mo distance of $\sim$ 2.8 Å is only slightly longer than the metal–metal distance in Mo metal (2.73 Å) or V metal (2.62 Å). This short distance should have a pronounced influence on the catalytic properties of the active site of $H_4[PVMo_{11}O_{40}] \times 13H_2O$ under reaction conditions, possibly on its capability to activate oxygen during the transition from the reduced form to the oxidized form. The coordination number of 0.6 determined for the V–Mo distance of $\sim$ 2.8 Å indicates either that not all Keggin ions exhibit a partial decomposition or that the V center in the lacunary Keggin ion is not always located in the vicinity of the extra-framework molybdenum. The former appears to be corroborated by the occupancy factor of the extra-Keggin site given in Table 2 ($\sim$ 0.9 Mo centers per Keggin ion).

The experimental data shown indicate that similar to observations of $H_3[PMo_{12}O_{40}] \times 13H_2O$, molybdenum centers migrate out of the Keggin ions of $H_4[PVMo_{11}O_{40}] \times 13H_2O$ onto extra-Keggin sites, whereas vanadium centers remain as V^{4+} in the partially decomposed lacunary Keggin ions of $Mo_x[PVMo_{11-x}O_{40}]$. In contrast to corresponding reports in the literature, thermal activation of $H_4[PVMo_{11}O_{40}] \times 13H_2O$ does not result in the majority of vanadium centers being located on extra-Keggin sites. Because in contrast to the treatment of $H_3[PMo_{12}O_{40}] \times 13H_2O$, a cubic phase stabilized by extra-Keggin metal centers can be readily obtained by a thermal treatment of $H_4[PVMo_{11}O_{40}] \times 13H_2O$, it has been concluded that V centers have to migrate out of the Keggin ion. [12] However, as we have previously demonstrated, a cubic HPOM with an X-ray diffraction pattern very similar to that of the cubic HPOM obtained from $H_4[PVMo_{11}O_{40}] \times 13H_2O$ can be prepared by thermal treatment of $H_3[PMo_{12}O_{40}] \times 13H_2O$ [9]. Hence, vanadium as an addenda substituent in the Keggin ion is not a prerequisite for the formation of a cubic HPOM. Based on NMR and ESR data for a thermally treated V-containing HPOM, Pöppl et al. suggested that V is situated on extra-Keggin sites [33]. However, from their NMR/ESR measurements the authors also report that already in the starting material vanadium centers are located outside the Keggin ions. Unfortunately, no further structural characterization of the vanadium-containing HPOM used is provided. Assuming that the authors did indeed prepare a vanadyl salt of $H_3[PMo_{12}O_{40}] \times 13H_2O$ (e.g., $(VO)[PMo_{12}O_{40}]$), the location of the V centers outside the Keggin ion in the thermally treated material is not surprising. However, the objective of the work presented here clearly was to study the influence of V centers substituting for Mo in regular molybdenum oxide on structure-activity correlations. This can only be achieved by an investigation of the structural evolution of $H_4[PVMo_{11}O_{40}] \times 13H_2O$ under reaction conditions instead of the evolution of $(VO)[PMo_{12}O_{40}]$.

The V K-near-edge regions of as-prepared $Cs_2H_2[PVMo_{11}O_{40}]$ and the thermally activated $Cs_2Mo_x[PVMo_{11-x}O_{40}]$ (not shown) are very similar to those measured for $H_4[PVMo_{11}O_{40}] \times 13H_2O$ and $Mo_x[PVMo_{11-x}O_{40}]$. This indicates a comparable local structure around the V centers in the Cs compounds (i.e., V located in the Keggin ion). However, because of the overlapping V K- and Cs L-edges, no detailed EXAFS analysis can be performed. The Cs L-edge spectra measured for the as-prepared $Cs_2H_2[PVMo_{11}O_{40}]$ and the thermally activated $Cs_2Mo_x[PVMo_{11-x}O_{40}]$ show no significant differences. This indicates that the void between the Keggin ions in $Cs_2H_2[PVMo_{11}O_{40}]$ is entirely filled by the Cs cations, and, hence, no migration of Mo into the close vicinity of the Cs ions is detectable. Hence, the stabilizing effect of Cs cations on the structural integrity of HPOM results from the occupation of extra-Keggin sites, which otherwise would be available for the migration of molybdenum centers out of the Keggin ions. This holds for the stabilizing effect of Cs in both $H_3[PMo_{12}O_{40}] \times 13H_2O$ and $H_4[PVMo_{11}O_{40}] \times 13H_2O$. Accordingly, the slow deactivation of heteropolyoxomolybdates under partial oxidation reaction conditions can be explained by the absence of this stabilization and, thus, the formation of interconnected species and, eventually, MoO_3 during thermal treatment.

4.3. *Thermal activation of $H_4[PVMo_{11}O_{40}] \times 13H_2O$ in propene and oxygen*

The structural changes observed in $H_4[PVMo_{11}O_{40}] \times 13H_2O$ during activation in propene and oxygen indicate a partial reduction (Fig. 11) and partial decomposition of the Keggin ions (Fig. 12) similar to the structural evolution that occurred during treatment of $H_4[PVMo_{11}O_{40}] \times 13H_2O$ in propene (Fig. 8). Apparently, the onset of the formation of a lacunary Keggin ion and the migration of Mo centers is correlated with the onset of catalytic activity. Similar to the structural behavior of $H_3[PMo_{12}O_{40}] \times 13H_2O$ under reaction conditions [9], a partial decomposition and formation of lacunary Keggin ions from $H_4[PVMo_{11}O_{40}] \times 13H_2O$ are prerequisites for the material to become an active partial oxidation catalyst. The genuine Mo site in the intact Keggin ion as it is present in the thermally stable $Cs_3[PMo_{12}O_{40}]$ under propene and oxygen at 673 K is catalytically inactive [9]. Only the partial decomposition of the Keggin ion and subsequent migration of molybdenum on vacant extra-Keggin sites turn the precursor Keggin ion in the HPOM into an active partial oxidation catalyst. Whereas the amplitude of the structural changes in the Keggin ion under reaction conditions is very similar for $H_4[PVMo_{11}O_{40}] \times 13H_2O$ and $H_3[PMo_{12}O_{40}] \times 13H_2O$ (Fig. 12), the evolution of the

electronic structure suggests a more pronounced reduction of the average Mo valence in $H_4[PVMo_{11}O_{40}] \times 13H_2O$ compared with $H_3[PMo_{12}O_{40}] \times 13H_2O$. Hence, in addition to a possible structure-promoting effect of V centers in molybdenum-based oxides, the amount of Mo centers with an average valence less than 6 appeared to increase in V-containing molybdenum oxides during activation in propene and oxygen. The latter seems to correlate with the improved catalytic activity observed (Fig. 11).

The catalytic activity and stability of the cubic $Mo_x[PVMo_{11-x}O_{40}]$ phase obtained from $H_4[PVMo_{11}O_{40}] \times 13H_2O$ was investigated by in situ XRD and XAS under propene oxidation conditions. It can be seen from Fig. 13 that the long-range order structure of the cubic phase persists to about 620 K in propene and oxygen. This structural stability under reaction conditions is unusual for as-prepared HPOMs, which tend to exhibit several transitions and decompositions during thermal treatment. The onset of catalytic activity of the cubic phase at about 573 K (Fig. 13B) is not accompanied by detectable changes in the long-range order structure. Both the stability under reaction conditions and the structural invariance at the onset of catalytic activity indicate that the structure of the cubic $Mo_x[PVMo_{11-x}O_{40}]$ is closely related to the structure of the active phase of $H_4[PVMo_{11}O_{40}] \times 13H_2O$. At temperatures above ~ 650 K the cubic phase exhibits a change in the relative ratio of the diffraction peaks around 20° and the occurrence of additional peaks, indicating the formation of an unidentified phase at elevated temperature. The modified cubic phase present above 650 K can still be simulated by the structure displayed in Fig. 7B, and a slightly elongated distance of the extra-Keggin Mo center from the Keggin ion can account for the modified peak ratio.

In contrast to the invariance of the long-range structure of $Mo_x[PVMo_{11-x}O_{40}]$ under reaction conditions, the short-range structure of the Keggin ion as detected by in situ XAS exhibits pronounced changes that correlate with the onset of catalytic activity at ~ 573 K. The structural changes observed are on the order of $\sim 5\%$ pointing towards a fine tuning of the Mo–O distances possibly accompanying the uptake of oxygen and the transition from the reduced form of the active phase to the oxidized form under reaction conditions. The resulting active site of these catalysts consists of an extra-framework molybdenum center that forms an oxo cluster together with the lacunary Keggin ion, presenting a coordinatively unsaturated metal center to the gas phase embedded in a matrix of stable terminal oxygen atoms (Fig. 15). The remaining hole in the lacunary Keggin ion permits adsorbed substrate molecules to access the bridging oxygen atoms in the vicinity of the Mo center. As can be seen from the correlation between local structural changes and the gas-phase composition in Fig. 14, the structural state of the reduced form of $Mo_x[PVMo_{11-x}O_{40}]$ can be reversibly altered by a change of the gas phase composition from propene and oxygen to propene. Apparently, at temperatures above ~ 600 K the oxygen coordinated to the active site of $Mo_x[PVMo_{11-x}O_{40}]$ can easily be exchanged and can participate in partial oxidation reactions, possibly according to a simple Langmuir–Hinshelwood mechanism. Future V *K*-edge XAFS investigations will be based on the established structural evolution of $H_4[PVMo_{11}O_{40}] \times 13H_2O$ during thermal activation and the detailed local coordination of the V centers in the resulting cubic $Mo_x[PVMo_{11-x}O_{40}]$, to reveal the dynamic behavior of the active site under varying reaction conditions.

4.4. Implication of V centers in molybdenum oxide-based catalysts for structure-activity relationships

The investigations presented indicate that HPOMs are indeed suitable three-dimensional model systems for the investigation of the directing effect of metal centers on the structural evolution of molybdenum oxides during thermal treatment. However, similar to the behavior of $H_3[PMo_{12}O_{40}] \times 13H_2O$, the original structure of as-prepared $H_4[PVMo_{11}O_{40}] \times 13H_2O$ does not correspond to the structure of the material under the reaction conditions. Instead, $H_4[PVMo_{11}O_{40}] \times 13H_2O$ should be regarded as the precursor of the catalytically active phase. The onset temperature of catalytic activity of $H_4[PVMo_{11}O_{40}] \times 13H_2O$ at ~ 573 K is in good agreement with that of $H_3[PMo_{12}O_{40}] \times 13H_2O$, MoO_3, $(Mo,V)_5O_{14}$, and other mixed-metal oxides (e.g., $MoVNbTeO_x$), indicating the formation of similar active sites on these materials under reaction conditions. The incorporation of V centers in the Keggin ion does not cause a pronounced destabilization of the Keggin ion and an accelerated decomposition at elevated temperatures. Apparently, vanadium centers are quite stable in the lacunary Keggin ion of $Mo_x[PVMo_{11-x}O_{40}]$ that forms under reaction conditions. Moreover, V centers can change their oxidation state from V^{5+} to V^{4+} without a significant detectable destabilization of the lacunary Keggin ion. The capability of V centers to substitute for Mo in as-prepared Keggin-type HPOMs and thermally activated HPOMs may be explained by the similar ion radii of V^{5+} (68 pm) and V^{4+} (72 pm) compared with Mo^{6+} (74 pm) in a sixfold coordination [34]. This is in contrast to the incorporation of larger Nb centers in HPOMs, which results in a pronounced destabilization of the Keggin ion [35]. Hence, vanadium may act as a structural promoter in the catalyst precursor facilitating the formation of the active (Mo, V) oxide phase. In addition to acting as a structural promoter, the structural flexibility and redox capability of the vanadium centers may facilitate a direct participation of V in the activation of gas-phase oxygen and propene on the active site of $Mo_x[PVMo_{11-x}O_{40}]$. The detailed investigations of the local structure of vanadium in $Mo_x[PVMo_{11-x}O_{40}]$ presented here permit for the first time the proposal of a model for the characteristic geometric structure of the active site in Mo- and V-containing metal oxide catalysts (Fig. 15). This structure deviates significantly from the structure of the as-prepared materials and could have by no means been inferred from it. In situ investigations are indispensable to

the elucidation of the "real structure" of a working catalyst under reaction conditions. Obviously, structure-activity correlations deduced from the ideal crystallographic structure of more complex Mo- and V-containing mixed-oxide catalysts have to be carefully validated by in situ bulk structural investigations.

5. Conclusions

The bulk structural evolution of $H_4[PVMo_{11}O_{40}] \times 13H_2O$ under reducing (propene) and partial oxidation reaction conditions (propene and oxygen) was studied by in situ XRD and XAS. During treatment in propene, the loss of crystal water in the temperature range from 373 to 573 K is followed by a partial decomposition, reduction of the average Mo valence, and formation of a characteristic cubic HPOM ($Mo_x[PVMo_{11-x}O_{40}]$) at 573 K. This behavior is similar to the structural evolution of $H_3[PMo_{12}O_{40}] \times 13H_2O$ during treatment in propene. The formation of cubic $Mo_x[PVMo_{11-x}O_{40}]$ with Mo centers on extra-Keggin framework positions and V centers remaining in the lacunary Keggin ions coincides with the onset of catalytic activity at $\sim$ 573 K. The detailed investigations of the local structure of vanadium in $Mo_x[PVMo_{11-x}O_{40}]$ presented here make it possible to propose a model for the geometric structure of the active site in Mo- and V-containing metal oxide catalysts. The cubic $Mo_x[PVMo_{11-x}O_{40}]$ phase prepared from $H_4[PVMo_{11}O_{40}] \times 13H_2O$ is stable in propene and oxygen up to $\sim$ 620 K and exhibits an onset of activity at $\sim$ 573 K. This onset of activity is correlated with characteristic changes in the average local Mo structure, indicating a reversible transition from the reduced state of the active site in $Mo_x[PVMo_{11x}O_{40}]$ to an oxidized state under propene oxidation reaction conditions.

Acknowledgments

We are grateful to the Hamburger Synchrotronstrahlungslabor (HASYLAB) and the European Synchrotron Radiation Facility (ESRF) for providing beamtime for the work described. R.E. Jentoft is acknowledged for participating in the XAS measurements. Prof. R. Schlögl is acknowledged for his continuous support.

References

[1] M.M. Lin, Appl. Catal. A: Gen. 207 (2001) 1.
[2] P. DeSanto Jr., D.J. Buttrey, R.K. Grasselli, C.G. Lugmair, A.F. Volpe, B.H. Toby, T. Vogt, Top. Catal. 23 (2003) 23.
[3] T. Okuhara, N. Mizuno, M. Misono, Adv. Catal. 41 (1996) 113.
[4] J.H. Holles, C.J. Dillon, J.A. Labinger, M.E. Davis, J. Catal. 218 (2003) 42;
J.H. Holles, C.J. Dillon, J.A. Labinger, M.E. Davis, J. Catal. 218 (2003) 54.
[5] J.B. Moffat, Metal–Oxygen Cluster: The Surface and Catalytic Properties of Heteropolyoxometalates, Kluwer-Academic–Plenum, New York, 2001.
[6] J.J. Borras-Almenar, E. Coronado, A. Muller, M.T. Pope (Eds.), Polyoxometalate Molecular Science, Kluwer, Dordrecht, The Netherlands, 2003.
[7] O. Watzenberger, G. Emig, D.T. Lynch, J. Catal. 124 (1990) 247.
[8] K.E. Lee, J. Melsheimer, S. Berndt, G. Mestl, R. Schlögl, K. Köhler, Appl. Catal. A: Gen. 214 (2001) 125.
[9] J. Wienold, O. Timpe, T. Ressler, Chem. Eur. J. 9 (2003) 6007.
[10] C. Marchal-Roch, N. Laronze, N. Guilou, A. Teze, G. Herve, Appl. Catal. A: Gen. 199 (2000) 33.
[11] C. Marchal-Roch, R. Bayer, J.F. Moisan, A. Teze, G. Herve, Top. Catal. 3 (1996) 407.
[12] T. Ilkenhans, B. Herzog, T. Braun, R. Schlögl, J. Catal. 153 (1995) 275.
[13] C. Marchal-Roch, J.-M.M. Millet, C.R. Acad. Sci. C 4 (2001) 321.
[14] G. Centi, V. Lena, F. Trifiro, D. Ghoussoub, C.F. Aissi, M. Guelton, J.P. Bonnelle, J. Chem. Soc. Faraday Trans. 86 (1990) 2775.
[15] F. Cavani, E. Etienne, R. Mezzogori, A. Pigamo, F. Trifiro, Catal. Lett. 75 (2001) 99.
[16] F. Cavani, R. Mezzogori, A. Pigamo, F. Trifiro, E. Etienne, Catal. Today 71 (2001) 97.
[17] L. Marosi, G. Cox, A. Tenten, H. Hibst, J. Catal. 194 (2000) 140.
[18] L. Marosi, C. Otero Arean, J. Catal. 213 (2003) 235.
[19] R. Bayer, C. Marchal-Roch, F.X. Liu, A. Teze, G. Herve, J. Mol. Catal. A: Chem. 110 (1996) 65.
[20] S. Albonetti, F. Cavani, F. Trifiro, M. Gazzano, M. Koutyrev, F.C. Aissi, A. Aboukais, M. Guelton, J. Catal. 146 (1994) 491.
[21] F.C. Jentoft, S. Klokishner, J. Kröhnert, J. Mehlsheimer, T. Ressler, O. Timpe, J. Wienold, R. Schlögl, Appl. Catal. A: Gen. 256 (2003) 291.
[22] G. Mestl, T. Ilkenhans, D. Spielbauer, M. Dieterle, O. Timpe, J. Kröhnert, F. Jentoft, H. Knözinger, R. Schlögl, Appl. Catal. A: Gen. 210 (2001) 13.
[23] T. Ressler, R.E. Jentoft, J. Wienold, M.M. Günter, O. Timpe, J. Phys. Chem. B 104 (2000) 6360.
[24] Designed by M. Hagelstein, T. Neisius, et al., ESRF, France, in a collaborative effort with the Fritz-Haber-Institut, Berlin, Germany.
[25] T. Ressler, J. Synch. Rad. 5 (1998) 118.
[26] D.C. Koningsberger, R. Prins, X-Ray Absorption Spectroscopy, Chemical Analysis, vol. 92, Wiley, New York, 1988.
[27] J.J. Rehr, C.H. Booth, F. Bridges, S.I. Zabinsky, Phys. Rev. B 49 (1994) 12347.
[28] T. Ressler, S.L. Brock, J. Wong, S.L. Suib, J. Phys. Chem. B 103 (1999) 6407.
[29] T. Ressler, R.E. Jentoft, J. Wienold, T. Neisius, J. Catal. 210 (2002) 67.
[30] T. Ressler, J. Wienold, R.E. Jentoft, F. Girgsdies, Eur. J. Inorg. Chem. 2 (2003) 301.
[31] J. Wong, F.W. Lytle, R.P. Messmer, D.H. Maylotte, Phys. Rev. B 30 (1984) 5596.
[32] J.K. Lee, V. Russo, J. Mehlsheimer, K. Köhler, R. Schlögl, Phys. Chem. Chem. Phys. 2 (2000) 2977.
[33] A. Pöppl, P. Manikandan, K. Köhler, P. Maas, P. Strauch, R. Böttcher, D. Goldfarb, J. Am. Chem. Soc. 123 (2001) 4577.
[34] M. Binnewies, M. Jaeckel, H. Willner, G. Rayner-Canham, Allgemeine und Anorganische Chemie, Spektrum, Heidelberg, 2004, according to ion radii assembled by Shannon and Prewitt with $d(O^{2-}) = 126$ pm.
[35] T. Ressler, O. Timpe, F. Girgsdies, Z. Kristallogr. (2005), in press.